Article

Surface Interactions and Quantum Kinetic Molecular Sieving for H and D Adsorption on a Mixed Metal#Organic Framework Material

Banglin Chen, Xuebo Zhao, Apipong Putkham, Kunlun Hong, Emil B. Lobkovsky, Eric J. Hurtado, Ashleigh J. Fletcher, and K. Mark Thomas

J. Am. Chem. Soc., **2008**, 130 (20), 6411-6423 • DOI: 10.1021/ja710144k • Publication Date (Web): 25 April 2008

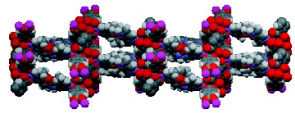

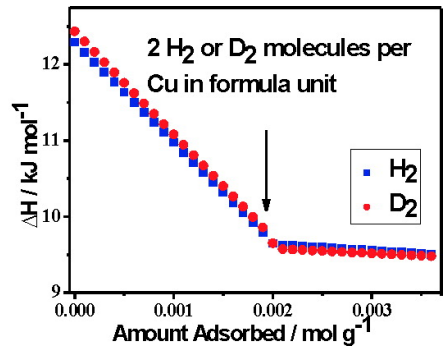

More About This Article

Additional resources and features associated with this article are available within the HTML version:

- Supporting Information
- Links to the 7 articles that cite this article, as of the time of this article download
- Access to high resolution figures
- Links to articles and content related to this article
- Copyright permission to reproduce figures and/or text from this article

View the Full Text HTML

J|A|C|S
ARTICLES

Published on Web 04/25/2008

Surface Interactions and Quantum Kinetic Molecular Sieving for H_2 and D_2 Adsorption on a Mixed Metal−Organic Framework Material

Banglin Chen,*,‡ Xuebo Zhao,† Apipong Putkham,† Kunlun Hong,⊥ Emil B. Lobkovsky,§ Eric J. Hurtado,‡ Ashleigh J. Fletcher,† and K. Mark Thomas*,†

Northern Carbon Research Laboratories, Sir Joseph Swan Institute for Energy Research and School of Chemical Engineering and Advanced Materials, Bedson Building, University of Newcastle upon Tyne, Newcastle upon Tyne, NE1 7RU, United Kingdom, Department of Chemistry, University of Texas-Pan American, Edinburg, Texas 78539, Department of Chemistry and Biology, Baker Laboratory, Cornell University, Ithaca, New York 14853-1301, and Chemical Sciences Divisions and Center for Nanophase Material Sciences (CNMS), Oak Ridge National Laboratory, Oak Ridge, Tennessee 3783

Received November 19, 2007; E-mail: mark.thomas@ncl.ac.uk; banglin@utpa.edu

Abstract: A rational strategy has been used to immobilize open metal sites in ultramicroporosity for stronger binding of multiple H_2 molecules per unsaturated metal site for H_2 storage applications. The synthesis and structure of a mixed zinc/copper metal−organic framework material $Zn_3(BDC)_3[Cu(Pyen)]\cdot(DMF)_5(H_2O)_5$ (H_2BDC = 1,4 benzenedicarboxylic acid and $PyenH_2$ = 5-methyl-4-oxo-1,4-dihydro-pyridine-3-carbaldehyde) is reported. Desolvation provides a bimodal porous structure $Zn_3(BDC)_3[Cu(Pyen)]$ (M′MOF **1**) with narrow porosity (<0.56 nm) and an array of pores in the *bc* crystallographic plane where the adsorbate–adsorbent interactions are maximized by both the presence of open copper centers and overlap of the potential energy fields from pore walls. The H_2 and D_2 adsorption isotherms for M′MOF **1** at 77.3 and 87.3 K were reversible with virtually no hysteresis. Methods for determination of the isosteric enthalpies of H_2 and D_2 adsorption were compared. A virial model gave the best agreement (average deviation <1 standard deviation) with the isotherm data. This was used in conjunction with the van't Hoff isochore giving isosteric enthalpies at zero surface coverage of 12.29 ± 0.53 and 12.44 ± 0.50 kJ mol^{-1} for H_2 and D_2 adsorption, respectively. This is the highest value so far observed for hydrogen adsorption on a porous material. The enthalpy of adsorption, decreases with increasing amount adsorbed to 9.5 kJ mol^{-1} at ∼1.9 mmol g^{-1} (2 H_2 or D_2 molecules per Cu corresponding to adsorption on both sides of planar Cu open centers) and is virtually unchanged in the range 1.9−3.6 mmol g^{-1}. Virial analysis of isotherms at 87.3 K is also consistent with two H_2 or D_2 molecules being bound to each open Cu center. The adsorption kinetics follow a double exponential model, corresponding to diffusion along two types of pores, a slow component with high activation energy (13.35 ± 0.59 kJ mol^{-1}) for the narrow pores and a faster component with low activation energy (8.56 ± 0.41 kJ mol^{-1}). The D_2 adsorption kinetic constants for both components were significantly faster than the corresponding H_2 kinetics for specific pressure increments and had slightly lower activation energies than the corresponding values for H_2 adsorption. The kD_2/kH_2 ratio for the slow component was 1.62 ± 0.07, while the fast component was 1.38 ± 0.04 at 77.3 K, and the corresponding ratios were smaller at 87.3 K. These observations of kinetic isotope quantum molecular sieving in porous materials are due to the larger zero-point energy for the lighter H_2, resulting in slower adsorption kinetics compared with the heavier D_2. The results show that a combination of open metal centers and confinement in ultramicroporosity leads to a high enthalpy for H_2 adsorption over a wide range of surface coverage and quantum effects influence diffusion of H_2 and D_2 in pores in M′MOF **1**.

1. Introduction

Porous materials, such as zeolites and activated carbons, are widely used for gas storage, purification, and separation, as catalysts and catalyst supports, and for adsorption of environmentally unfriendly species. In the past decade, strategies have been developed for the design and synthesis of porous metal−organic framework materials (MOFs) with a wide range of structures using secondary building units. These materials have many design possibilities and, in addition, well-defined porous structures and surface sites, which may be varied systematically for possible specific applications in materials science.[1,2] MOFs may have unique structural characteristics, for

† University of Newcastle upon Tyne.
‡ University of Texas-Pan American.
§ Cornell University.
⊥ Oak Ridge National Laboratory.

(1) Kepert, C. J. *Chem. Commun.* **2006**, *7*, 695–700.
(2) Horike, S.; Matsuda, R.; Tanaka, D.; Mizuno, M.; Endo, K.; Kitagawa, S. *J. Am. Chem. Soc.* **2006**, *128*, 4222–4223.

example, chiral structures,[3–9] and flexibility, allowing distortion during the adsorption process by a scissoring mechanism.[10–12] Porous MOFs with selectivity for various species,[13] fluorescence[14,15] and luminescence[3,4,7,16–21] characteristics, and magnetic[22–24] properties, have been synthesized. MOFs have also been prepared that exhibit reversible vapochromic behavior,[25] and enantioselective adsorption[5,6] and act as photocatalysts.[26] The possibility of producing MOFs with a wide range of structures and properties will lead to the development of new functional materials with many potential applications such as gas storage,[27–34] gas separation,[35–41] solution-separation processes,[42–46] catalysis,[26,36,47–51] and as sensors.[52–57] The ability to rationally design MOFs leads to the possibility of optimizing pore structure, surface chemistry, and other properties for specific applications.

Hydrogen storage has been identified as the key factor limiting the future development of the hydrogen economy for emission-free transport applications. Hydrogen adsorption on porous materials has been proposed as a method for hydrogen storage for transport applications.[58] Recent studies have shown that 6–8 wt % of hydrogen can be adsorbed on porous carbons and metal−organic framework materials at 77 K.[33,59–62] The marked decrease in H_2 adsorption with increasing temperature is the

(3) Lu, Z.; Wen, L.; Ni, Z.; Li, Y.; Zhu, H.; Meng, Q. *Cryst. Growth Desm* **2007**, *7*, 268–274.
(4) Fang, Q.; Zhu, G.; Xue, M.; Sun, J.; Sun, F.; Qiu, S. *Inorg. Chem.* **2006**, *45*, 3582–3587.
(5) Dybtsev, D. N.; Nuzhdin, A. L.; Chun, H.; Bryliakov, K. P.; Talsi, E. P.; Fedin, V. P.; Kim, K. *Angew. Chem., Int. Ed.* **2006**, *45*, 916–920.
(6) Vaidhyanathan, R.; Bradshaw, D.; Rebilly, J. N.; Barrio, J. P.; Gould, J. A.; Berry, N. G.; Rosseinsky, M. J. *Angew. Chem., Int. Ed.* **2006**, *45*, 6495–6499.
(7) Petoud, S.; Muller, G.; Moore, E. G.; Xu, J.; Sokolnicki, J.; Riehl, J. P.; Le, U. N.; Cohen, S. M.; Raymond, K. N. *J. Am. Chem. Soc.* **2007**, *129*, 77–83.
(8) Kaneko, W.; Kitagawa, S.; Ohba, M. *J. Am. Chem. Soc.* **2007**, *129*, 248–249.
(9) Sun, D.; Ke, Y.; Collins, D. J.; Lorigan, G. A.; Zhou, H. C. *Inorg. Chem.* **2007**, *46*, 2725–2734.
(10) Fletcher, A. J.; Cussen, E. J.; Prior, T. J.; Rosseinsky, M. J.; Kepert, C. J.; Thomas, K. M. *J. Am. Chem. Soc.* **2001**, *123*, 10001–10011.
(11) Fletcher, A. J.; Cussen, E. J.; Bradshaw, D.; Rosseinsky, M. J.; Thomas, K. M. *J. Am. Chem. Soc.* **2004**, *126*, 9750–9759.
(12) Fletcher, A. J.; Thomas, K. M.; Rosseinsky, M. J. *J. Solid State Chem.* **2005**, *178*, 2491–2510.
(13) Llewellyn, P. L.; Bourrrelly, S.; Serre, C.; Filinchuk, Y. G. F. *Angew. Chem., Int. Ed.* **2006**, *45*, 7751–7754.
(14) Feng, W.; Xu, Y.; Zhou, G.; Zhang, C.; Zheng, X. *Inorg. Chem. Commun.* **2007**, *10*, 49–52.
(15) Zou, R. Q.; Yamada, Y.; Xu, Q. *Microporous Mesoporous Mater.* **2006**, *91*, 233–237.
(16) Chandler, B. D.; Cramb, D. T.; Shimizu, G. K. H. *J. Am. Chem. Soc.* **2006**, *128*, 10403–10412.
(17) Pelle, F.; Surble, S.; Serre, C.; Millange, F.; Ferey, G. *J. Lumin.* **2007**, *122–123*, 492–495.
(18) Sun, D.; Ma, S.; Ke, Y.; Petersen, T. M.; Zhou, H. C. *Chem. Commun.* **2005**, *21*, 2663–2665.
(19) Bauer, C. A.; Timofeeva, T. V.; Settersten, T. B.; Patterson, B. D.; Liu, V. H.; Simmons, B. A.; Allendorf, M. D. *J. Am. Chem. Soc.* **2007**, *129*, 7136–7144.
(20) Song, Y. S.; Yan, B.; Chen, Z. X. *J. Solid State Chem.* **2006**, *179*, 4037–4046.
(21) Guo, X.; Zhu, G.; Sun, F.; Li, Z.; Zhao, X.; Li, X.; Wang, H.; Qiu, S. *Inorg. Chem.* **2006**, *45*, 2581–2587.
(22) Shiga, T.; Okawa, H.; Kitagawa, S.; Ohba, M. *J. Am. Chem. Soc.* **2006**, *128*, 16426–16427.
(23) Neville, S. M.; Moubaraki, B.; Murray, K. S.; Kepert, C. J. *Angew. Chem., Int. Ed.* **2007**, *46*, 2059–2062.
(24) Yanai, N.; Kaneko, W.; Yoneda, K.; Ohba, M.; Kitagawa, S. *J. Am. Chem. Soc.* **2007**, *129*, 3496–3497.
(25) Wadas, T. J.; Wang, Q.-M.; Kim, Y.-J.; Flaschenreim, C.; Blanton, T. N.; Eisenberg, R. *J. Am. Chem. Soc.* **2004**, *126*, 16841–16849.
(26) Mahata, P.; Madras, G.; Natarajan, S. *J Phys. Chem. B* **2006**, *110*, 13759–13768.
(27) Zhao, X.; Xiao, B.; Fletcher, A. J.; Thomas, K. M.; Bradshaw, D.; Rosseinsky, M. J. *Science* **2004**, *306*, 1012–1015.
(28) Rosi, N. L.; Eckert, J.; Eddaoudi, M.; Vodak, D. T.; Kim, J.; O'Keeffe, M.; Yaghi, O. M. *Science* **2003**, *300*, 1127–1129.
(29) (a) Ferey, G.; Mellot-Draznieks, C.; Serre, C.; Millange, F.; Dutour, J.; Surble, S.; Margiolaki, I. A. *Science* **2005**, *309*, 2040–2042. (b) Ferey, G.; Mellot-Draznieks, C.; Serre, C.; Millange, F.; Dutour, J.; Surble, S.; Margiolaki, I. A. *Science* **2005**, *310*, 1119.
(30) Rowsell, J. L. C.; Yaghi, O. M. *Angew. Chem., Int. Ed.* **2005**, *44*, 4670–4679.
(31) Chun, H.; Dybtsev, D. N.; Kim, H.; Kim, K. *Chem. Eur. J.* **2005**, *11*, 3521–3529.
(32) Sun, D.; Ma, S.; Ke, Y.; Collins, D. J.; Zhou, H. C. *J. Am. Chem. Soc.* **2006**, *128*, 3896–3897.
(33) Thomas, K. M. *Catal. Today* **2007**, *120*, 389–398.
(34) Mulfort, K. L.; Hupp, J. T. *J. Am. Chem. Soc.* **2007**, *129*, 9604–9605.
(35) Pan, L.; Olson, D. H.; Ciemnolonski, L. R.; Heddy, R.; Li, J. *Angew. Chem., Int. Ed.* **2006**, *45*, 616–619.
(36) Pan, L.; Adams, K. M.; Hernandez, H. E.; Wang, X.; Zheng, C.; Hattori, Y.; Kaneko, K. *J. Am. Chem. Soc.* **2003**, *125*, 3062–3067.
(37) Dybtsev, D. N.; Chun, H.; Yoon, S. H.; Kim, D.; Kim, K. *J. Am. Chem. Soc.* **2004**, *126*, 32–33.
(38) Atwood, J. L.; Barbour, L. J.; Jerga, A. *Angew. Chem., Int. Ed.* **2004**, *43* (22), 2948–2950.
(39) Dinca, M.; Long, J. R. *J. Am. Chem. Soc.* **2005**, *127*, 9376–9377.
(40) Matsuda, R.; Kitaura, R.; Kitagawa, S.; Kubota, Y.; Belosludov, R. V.; Kobayashi, T. C.; Sakamoto, H.; Chiba, T.; Takata, M.; Kawazoe, Y.; Mita, Y. *Nature (London, United Kingdom)* **2005**, *436*, 238–241.
(41) Bourrelly, S.; Llewellyn, P. L.; Serre, C.; Millange, F.; Loiseau, T.; Ferey, G. *J. Am. Chem. Soc.* **2005**, *127*, 13519–13521.
(42) Maji, T. K.; Uemura, K.; Chang, H. C.; Matsuda, R.; Kitagawa, S. *Angew. Chem., Int. Ed.* **2004**, *43*, 3269–3272.
(43) Custelcean, R.; Gorbunova, M. G. *J. Am. Chem. Soc.* **2005**, *127*, 16362–16363.
(44) Chen, B.; Liang, C.; Yang, J.; Contreras, D. S.; Clancy, Y. L.; Lobkovsky, E. B.; Yaghi, O. M.; Dai, S. *Angew. Chem., Int. Ed.* **2006**, *45*, 1390–1393.
(45) Custelcean, R.; Haverlock, T. J.; Moyer, B. A. *Inorg. Chem.* **2006**, *45*, 6446–6452.
(46) Pan, L.; Parker, B.; Huang, X.; Olson, D. H.; Lee, J. Y.; Li, J. *J. Am. Chem. Soc.* **2006**, *128*, 4180–4181.
(47) Fujita, M.; Kwon, Y. J.; Washizu, S.; Ogura, K. *J. Am. Chem. Soc.* **1994**, *116*, 1151–1152.
(48) Seo, J. S.; Whang, D.; Lee, H.; Jun, S. I.; Oh, J.; Jeon, Y. J.; Kim, K. *Nature* **2000**, *404* (6781), 982–986.
(49) Hu, A.; Ngo, H. L.; Lin, W. C. *Angew. Chem., Int. Ed.* **2003**, *42*, 6000–6003.
(50) Hu, A.; Ngo, H. L.; Lin, W. *J. Am. Chem. Soc.* **2003**, *125*, 11490–11491.
(51) Lin, W. *J. Solid State Chem.* **2005**, *178*, 2486–2490.
(52) Albrecht, M.; Lutz, M.; Spek, A. L.; Koten, G. v. *Nature* **2000**, *406*, 970–974.
(53) Liu, W.; Jiao, T.; Li, Y.; Liu, Q.; Tan, M.; Wang, H.; Wang, L. *J. Am. Chem. Soc.* **2004**, *126*, 2280–2281.
(54) Zhao, B.; Chen, X.-Y.; Cheng, P.; Liao, D.-Y.; Yan, S.-P.; Jiang, Z.-H. *J. Am. Chem. Soc.* **2004**, *126*, 15394–15395.
(55) Lefebvre, J.; Batchelor, R. J.; Leznoff, D. B. *J. Am. Chem. Soc.* **2004**, *126*, 16117–16125.
(56) Zhao, B.; Gao, H.-L.; Chen, X.-Y.; Cheng, P.; Shi, W.; Liao, D.-Z.; Yan, S.-P.; Jiang, Z.-H. *Chem. Eur. J.* **2005**, *12*, 149–158.
(57) Chen, B.; Yang, Y.; Zapata, F.; Lin, G.; Qian, G.; Lobkovsky, E. B. *Adv. Mater.* **2007**, *19* (13), 1693–1696.
(58) Grand challenge for basic and applied research on hydrogen storage: statement of objectives. http://www1.eere.energy.gov/hydrogenandfuelcells/storage/nation_proj.html.
(59) Lin, X.; Jia, J.; Zhao, X.; Thomas, K. M.; Blake, A. J.; Walker, G. S.; Champness, N. R.; Hubberstey, P.; Schroder, M. *Angew. Chem., Int. Ed.* **2006**, *45*, 7358–7364.
(60) Wong-Foy, A. G.; Matzger, A. J.; Yaghi, O. M. *J. Am. Chem. Soc.* **2006**, *128*, 3494–3495.
(61) Dinca, M.; Dailly, A.; Liu, Y.; Brown, C. M.; Neumann, D. A.; Long, J. R. *J. Am. Chem. Soc.* **2006**, *128*, 16876–16883.
(62) Yang, Z.; Xia, Y.; Mokaya, R. *J. Am. Chem. Soc.* **2007**, *129*, 1673–1679.
(63) Kubas, G. J. *Proc. Natl. Acad. Sci. (US)* **2007**, *104*, 6901–6907.
(64) Chen, B.; Ockwig, N. W.; Millward, A. R.; Contreras, D. S.; Yaghi, O. M. *Angew. Chem., Int. Ed.* **2005**, *44*, 4745–4749.

current limitation on the use of these materials for vehicle storage applications,[33] but this can be improved by increasing the H_2−surface interaction.[63–65] The hydrogen−surface interaction is weak with the current maximum enthalpy of adsorption being 10.5 kJ mol^{-1}.[66]

If a porous material can bind hydrogen molecules by stronger interactions than nonspecific van der Waals interactions, but not strong enough to break the H_2 bond, it offers a possible hydrogen storage option with improved temperature characteristics. The side-on (η^2) bonding of H_2 to organometallic complexes primarily involves donation of two σ electrons to a vacant metal orbital.[63] The H_2 coordinated to the metal is typically 20% longer than in H_2 gas. This led to the proposal that H_2-open metal center interactions are stronger than other surface interactions in MOFs and these interactions may be tuned by varying the metal. Currently, only MOFs exist where unsaturated metal sites are a small fraction of the available surface area. Inelastic neutron scattering studies have shown that sites on the organic linker in MOFs have lower binding energies but greater surface area and H_2 capacities.[67] The hydrogen interaction with surfaces is also enhanced in pores with dimensions <0.6 nm by overlap of the potential energy fields from pore walls.

Quantum effects may be observed for H_2 and D_2 adsorption when the difference between the diameter of the molecule and the pore diameter becomes comparable to the de Broglie wavelength (λ). Quantum effects may significantly affect molecular transport in pores.[68–70] The de Broglie wavelengths for H_2 and D_2, under conditions of one-dimensional (1-D) flow in nanometer cylindrical pores, at 77 K are ~0.249 and 0.176 nm, respectively. Therefore, adsorption/desorption of H_2 and D_2 (size 0.24–0.31 nm) within <0.6 nm pores may involve quantum effects. Hence, at 77 K, an intrinsic conflict exists between narrowing the porosity to maximize the H_2−surface interactions and rapid diffusion into the adsorbent because quantum effects may influence diffusion along pores when the differences between the H_2 and pore diameters are similar to the de Broglie wavelength. The de Broglie wavelength decreases with increasing temperature, and hence quantum effects are not expected to be an issue for H_2 storage at ambient temperatures.

Limitations exist for the number of open metal centers that can be incorporated in MOFs to enhance H_2-surface interactions. Therefore, we have investigated the combination of planar structural features incorporating open metal centers for binding hydrogen molecules on both sides with confinement in ultramicroporosity, where the differences between H_2 and pore dimensions are close to the de Broglie wavelength. The emerging preconstructed building block approach was used to incorporate open copper centers coordinated to Pyen ligands (see Figure 1a) as pillars in an ultramicroporous mixed copper−zinc metal−organic framework. This is a possible future synthetic route to high-capacity hydrogen storage at higher temperatures through increasing hydrogen surface interactions in MOFs.[71–73] Relationships between surface chemistry, pore structural features and adsorption characteristics were studied to provide fundamental information on H_2−surface interactions for designing new materials. The relationship between H_2 and D_2 adsorption thermodynamics and stoichiometry suggested that there was a specific interaction between hydrogen and open metal centers. Confinement effects in the ultramicroporosity decreased diffusion of H_2 in pores, and the results are discussed in terms of quantum effects.

2. Experimental Section

2.1. Materials and Methods. 2.1.1. Reagents. All reagents and solvents employed in synthetic studies were commercially available and used as supplied without further purification.

2.1.2. Gases. Ultra-pure hydrogen (H_2 99.9999%, H_2O < 500 ppb, N_2 < 200 ppb, O_2 < 100 ppb, CO + CO_2 < 50 ppb, total hydrocarbons <50 ppb) was supplied by Air Products Ltd. Deuterium (99.98% D_2), was supplied by BOC Ltd.

2.1.3. Gas Purification. H_2 and D_2 were purified using a two stage process involving adsorption on a zeolite (calcium alumino silicate (1/16" pellets)) at 298 K to remove any water vapor present and activated carbon (G212, particle size 6 × 12 mesh) at 195 K to remove hydrocarbons and other gas impurities.[70]

2.2. Synthetic Studies. 5-Methyl-4-oxo-1, 4-dihydro-pyridine-3-carbaldehyde was synthesized according to the literature procedure.[74]

2.2.1. $Cu(PyenH_2)(NO_3)_2$. A solution of ethylenediamine (0.766 g, 12.75 mmol) in EtOH (20 mL) was added dropwise to a solution of 5-methyl-4-oxo-1, 4-dihydro-pyridine-3-carbaldehyde (3.09 g, 25.50 mmol) in EtOH (130 mL), and the resulting mixture was refluxed for two hours to form a clear light brown solution. To this solution, a solution of $Cu(NO_3)_2 \cdot 2.5\ H_2O$ (2.965 g, 12.75 mmol) in EtOH (20 mL) was added, forming a blue precipitate of $Cu(PyenH_2)(NO_3)_2$ that was collected by filtration, washed with EtOH and air-dried (4.12 g, 67%). Elemental analysis (%): Calcd. for $Cu(PyenH_2)(NO_3)_2$ ($C_{16}H_{18}N_6O_8Cu$): C, 39.55; H, 3.73; N, 17.29; Found: C, 38.74; H, 3.82; N, 16.85.

2.2.2. $Zn_3(BDC)_3[Cu(Pyen)] \cdot (DMF)_5(H_2O)_5$. (M′MOF **1**) A mixture of $Zn(NO_3)_2 \cdot 6H_2O$ (1.2116 g, 4.07 mmol), H_2BDC (0.6732 g, 4.06 mmol), and $Cu(PyenH_2)(NO_3)_2$ (0.600 g, 1.24 mmol) was dissolved in a mixture of DMF (306 mL) and H_2O (30.6 mL), and heated in a vial (400 mL) at 373 K for 24 h. The dark blue thin plates formed were collected and dried in air (0.75 g, 52%). Elemental analysis (%): Calcd. for $Zn_3(BDC)_3[Cu(Pyen)] \cdot (DMF)_5(H_2O)_5$ ($C_{55}H_{73}N_9O_{24}CuZn_3$): C, 43.92; H, 4.89; N, 8.38; Found: C, 43.67; H, 4.70; N, 8.51.

2.3. X-ray Crystallography. 2.3.1. Single-Crystal Studies. Intensity data for M′MOF **1** were collected using Bruker X8 APEX II diffractometer (Mo Kα radiation) in a cold nitrogen stream. Data collection and reduction were carried out using the Bruker Apex2 software package. Structures were solved by direct methods and refined by full-matrix least-squares, using SHELXL97. All non-hydrogen atoms were refined anisotropically. The electron density contribution of the diffuse scattering of the disordered guest molecules (DMF and H_2O) was handled using the SQUEEZE procedure in the PLATON software suite. Crystal data for M′MOF **1**: Formula $C_{40}H_{26}CuN_4O_{14}Zn_3$, monoclinic, space group $P(2_1/c)$, $a = 41.254(4)$, $b = 9.4592(9)$, $c = 18.4138(16)$ Å, $\beta = 98.645(3)°$,

(65) Forster, P. M.; Eckert, J.; Chang, J.-S.; Park, S.-E.; Férey, G.; Cheetham, A. K. *J. Am. Chem. Soc.* **2003**, *125*, 1309–1312.
(66) Dinca, M.; Long, J. R. *J. Am. Chem. Soc.* **2007**, *129*, 11172–11176.
(67) Rowsell, J. L. C.; Eckert, J.; Yaghi, O. M. *J. Am. Chem. Soc.* **2005**, *127*, 14904–14910.
(68) Beenakker, J. J. M.; Borman, V. D.; Krylov, S. Y. *Phys. Rev. Lett.* **1994**, *72*, 514–517.
(69) Beenakker, J. J. M.; Borman, V. D.; Krylov, S. Y. *Chem. Phys. Lett.* **1995**, *232*, 379–382.
(70) Zhao, X.; Villar-Rodil, S.; Fletcher, A. J.; Thomas, K. M. *J. Phys. Chem. B* **2006**, *110*, 9947–9955.
(71) Kitaura, R.; Onoyama, G.; Sakamoto, H.; Matsuda, R.; Noro, S.; Kitagawa, S. *Angew. Chem., Int. Ed.* **2004**, *43* (20), 2684–2687.
(72) Chen, B.; Fronczek, F. R.; Maverick, A. W. *Inorg. Chem.* **2004**, *43* (26), 8209–8211.
(73) Cho, S. H.; Ma, B.; Nguyen, S. T.; Hupp, J. T.; Albrecht-Schmitt, T. E. *Chem. Commun. (Cambridge, United Kingdom)* **2006**, *24*, 2563–2565.
(74) Arya, F.; Bouquant, J.; Chuche, J. *Synthesis* **1983**, *11*, 946–948.

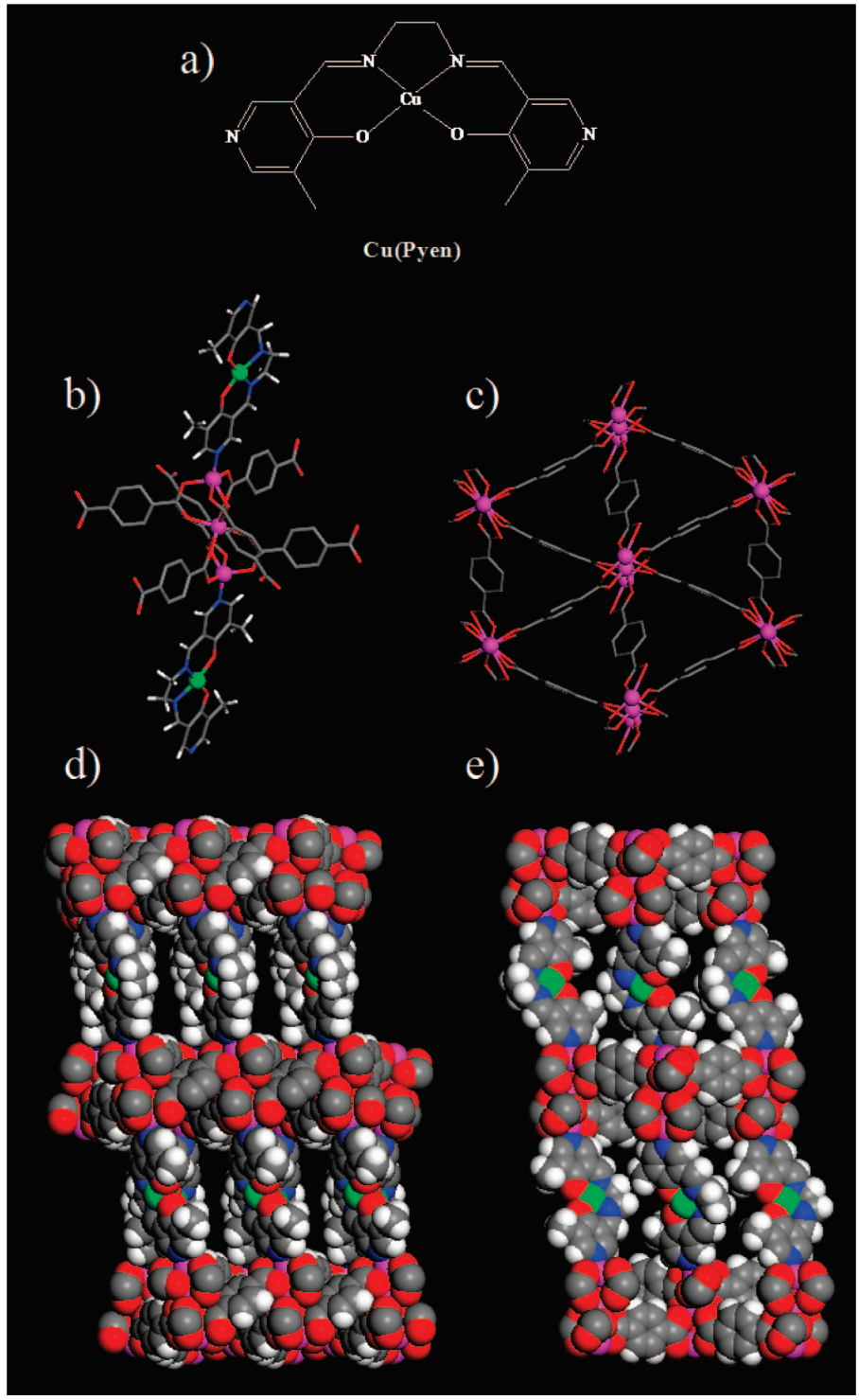

Figure 1. X-ray crystal structure of M′MOF **1** ($Zn_3(BDC)_3Cu(Pyen)$) showing (a) Pyen, (b) one trinuclear $Zn_3(COO)_6$ secondary building unit, (c) one 3^6 tessellated $Zn_3(BDC)_3$ 2-D sheet that is pillared by the Cu(Pyen) to form a 3-D microporous M′MOF **1** having (d) the curved pores of about 5.6 × 12.0 Å along the *c* axis and (e) the irregular ultramicropores along the *b* axis, respectively. Legend: Zn (magenta), Cu (green), O (red), N (blue), C (gray), H (white).

$V = 7103.9(11)$ Å^3, $Z = 4$, $D_{calc} = 0.978$ g cm^{-3}, $\mu = 1.338$ mm^{-1}, $T = 173$ K, R_1 [$I > 2\sigma(I)$] = 0.0456, wR_2 (all data) = 0.1324, S = 0.881.

2.3.2. Powder Diffraction Studies. Powder XRD patterns were obtained with a Scintag X1 powder diffractometer system using Cu Kα radiation with a variable divergent slit and a solid-state detector. The routine power was 1400 W (40 kV, 35 mA). Low-background quartz XRD slides (Gem Depot, Inc., Pittsburgh, PA) were used. For analyses, powder samples were dispersed on glass slides.

2.4. Adsorption Studies. The adsorption/desorption characteristics were studied using two Intelligent Gravimetric Analysers manufactured by Hiden Isochema Ltd., Warrington, UK. These instruments are ultra high vacuum, clean systems with diaphragm

and turbo pumping facilities, which are suitable for the measurement of adsorption kinetics of gases and vapors on porous materials.[70,75–77] The microbalances have a long-term stability of ±1 μg with a weighing resolution of 0.2 μg. The sample of methanol-exchanged M′MOF 1 was degassed at 343 K under ultra high vacuum (10^{-10} bar) until no further weight loss occurred prior to H_2 and D_2 adsorption. Pressure control changes were completed within ~15 s using a computer control algorithm. The pressure was monitored by three pressure transducers in both instruments. The low pressure (110 kPa) instrument had pressure transducers with ranges 0–0.2, 0–10 and 0–100 kPa. The high pressure (1 MPa) instrument had pressure transducers with ranges 0–0.2, 0–10 and 0–1000 kPa. Pressure was maintained at the set point by active computer control of inlet/outlet valves throughout the duration of the adsorption kinetic experiments. The accuracy of the set-point pressure regulation was ±0.02% of the range used. The mass relaxation to equilibrium was measured in real time and the approach to equilibrium was monitored using a computer algorithm. The algorithm calculates the equilibrium uptake from the mass uptake profile using the Linear Driving Force model throughout the mass relaxation process. The time origin of the fitted trend is also adjusted automatically so as to reject data at shorter time if they do not conform to the model. This adjustment is on the basis that the relaxation due to sorption will always tend to a single exponential trend in the long time limit. When the uptake reached the specified percentage of the calculated uptake the equilibrium was deemed to have been reached. A limit of 99.9% of total uptake for the pressure increment was used throughout this study. Both the sample and counterweight sides of the balance were cooled to liquid nitrogen or liquid argon temperatures for the H_2 and D_2 adsorption/desorption experiments in order to minimize buoyancy corrections and thermal transpiration effects. The measurement protocols used in this study were validated as described previously.[70]

The repeatabilities of the isotherm and kinetic measurements were established by a detailed series of measurements on M′MOF **1** at 77.3 and 87.3 K, and these are discussed in Results and Discussion.

2.4.1. Saturated Vapor Pressures. H_2 and D_2 were used above their critical temperatures. The saturated vapor pressures for the vapors were calculated using the following equation:[78]

$$\log_{10} p = A - \frac{B}{T + C} \quad (1)$$

where p is the saturated vapor pressure (Torr), T is the temperature in degrees Celsius and A, B, and C are constants defined by the adsorbate. The following values, with valid temperature ranges, were used: methanol (259–338 K): $A = 7.89750$, $B = 1474.08$, $C = 229.13$ and benzene (281–403 K): $A = 6.90565$, $B = 1211.033$, $C = 220.79$.

2.4.2. Thermogravimetric (TGA) Studies. TGA data were obtained on a Perkin-Elmer TGA 7 instrument with a heating rate of 5 K min^{-1} under N_2 atmosphere.

2.4.3. Scanning Electron Microscopy Studies. Scanning electron micrographs were obtained using a Hitachi S2400 Scanning Electron Microscope fitted with an Oxford Instruments Isis 200 ultra thin window X-ray detector.

3. Results and Discussion

The new Salen-type Schiff base of pyridine derivative $PyenH_2$ was prepared by condensation of 5-methyl-4-oxo-1, 4-dihydropyridine-3-carbaldehyde with ethylenediamine. Reaction of $Cu(NO_3)_2 \cdot 2.5H_2O$ with $PyenH_2$ formed the preconstructed building block $Cu(PyenH_2)(NO_3)_2$ that was easily incorporated into M′MOF **1** by self-assembly with $Zn(NO_3)_2 \cdot 6H_2O$ and H_2BDC in DMF/H_2O at 373 K as dark blue thin plates. It was formulated as $Zn_3(BDC)_3[Cu(Pyen)] \cdot (DMF)_5(H_2O)_5$ by elemental microanalysis and single-crystal X-ray diffraction studies, and the phase purity of the bulk material was independently confirmed by powder X-ray diffraction (PXRD).

Thermogravimetric analysis (TGA) of as-synthesized M′MOF **1** showed that it had a two step desolvation with a small initial weight loss of ~4 wt % at ~390 K with a second much larger step giving a stable porous structure (weight loss: 29.9 wt % at ~500 K; Calcd 30.3 wt %) (see Supporting Information). The desolvated M′MOF **1** for the adsorption studies was prepared from the methanol-exchanged M′MOF **1** by activation at 353 K under ultra-high vacuum. The XRD profile of desolvated M′MOF **1** indicates that it maintains the crystalline structure (see Supporting Information).

3.1. Structural Characteristics. The crystal structure of M′MOF **1** is a three-dimensional framework composed of the trinuclear $Zn_3(COO)_6$ secondary building units (Figure 1b). These SBUs are bridged by BDC anions to form the 3^6 tessellated $Zn_3(BDC)_3$ 2-D sheets (Figure 1c) that are further pillared by the Cu(Pyen) to construct a 3D framework. Desolvation produces rationally immobilized copper centers within the two types of micropores: curved pores of about 5.6 × 12.0 Å in the direction of the *c* crystallographic axis (Figure 1d, *c* pores) and irregular ultramicropores in the direction of the *b* crystallographic axis (Figure 1e, *b* pores). This gives an array of pores in the *bc* crystallographic plane. The copper sites have four of six possible coordination sites bound by Schiff base N and O, so that there are two potential open sites either side of the CuN_2O_2 plane for binding of hydrogen molecules.

3.2. Porous Structure Characterization. Nitrogen adsorption on M′MOF **1** at 77.3 K was very slow due to activated diffusion effects. Therefore, the porous structure of M′MOF **1** was characterized using methanol adsorption at 298 K. The isotherm is type IV in the IUPAC classification scheme[79] and has a small amount of hysteresis, as shown in Figure 2a. It is evident that there is a point of inflection at $p/p^0 = \sim 0.1$ before the plateau is reached. Linear extrapolation of the isotherm data for p/p^0: 0.48–0.96, was 6.339 ± 0.012 mmol g^{-1}. The uptake at 16 kPa ($p/p^0 = 0.96$) was 6.336 mmol g^{-1}. The pore volume calculated, using a density of 0.7914 g cm^{-3} for the adsorbed methanol phase,[78] was 0.257 ± 0.001 cm^3 g^{-1}.

Figure 2b shows the adsorption and desorption isotherms for benzene at 298 K. It is apparent that there is a plateau at 1.6−1.75 mmol g^{-1} (p/p^0: 0.05–0.24). This corresponds to adsorption of ~1.7 C_6H_6 molecules per $Zn_3(BDC)_3Cu(Pyen)$ formula unit. Hence, there is no relation of the plateau to stoichiometry. Above this relative pressure range there is a steep increase followed by a plateau. The shape is probably due to structural rearrangement to accommodate the extra benzene molecules in the pores.[80] Extrapolation of the plateau to $p/p^0 = 1$, gave amount adsorbed of 2.779 ± 0.012 mmol g^{-1} (2.9 C_6H_6 per $Zn_3(BDC)_3Cu(Pyen)$ formula unit). The pore volume calculated, using a density of adsorbed benzene of 0.8736 g cm^{-3},[78] was 0.248 ± 0.001 cm^3 g^{-1}.

(75) Harding, A. W.; Foley, N. J.; Norman, P. R.; Francis, D. C.; Thomas, K. M. *Langmuir* **1998**, *14*, 3858–3864.
(76) Foley, N. J.; Forshaw, P. L.; Thomas, K. M.; Stanton, D.; Norman, P. R. *Langmuir* **1997**, *13*, 2083–2089.
(77) Fletcher, A. J.; Thomas, K. M. *Langmuir* **1999**, *15*, 6908–6914.
(78) *CRC Handbook of Chemistry and Physics*, 74th ed.; The Chemical Rubber Co.: OH, 1993.
(79) Sing, K. S. W.; Everett, D. H.; Haul, R. A. W.; Moscou, L.; Pierotti, R. A.; Rouquerol, J.; Siemieniewska, T. *Pure Appl. Chem.* **1985**, *57*, 603–619.
(80) Uemura, K.; Yamasaki, Y.; Komagawa, Y.; Tanaka, K.; Kita, H. *Angew. Chem., Int. Ed.* **2007**, *46*, 6662–6665.

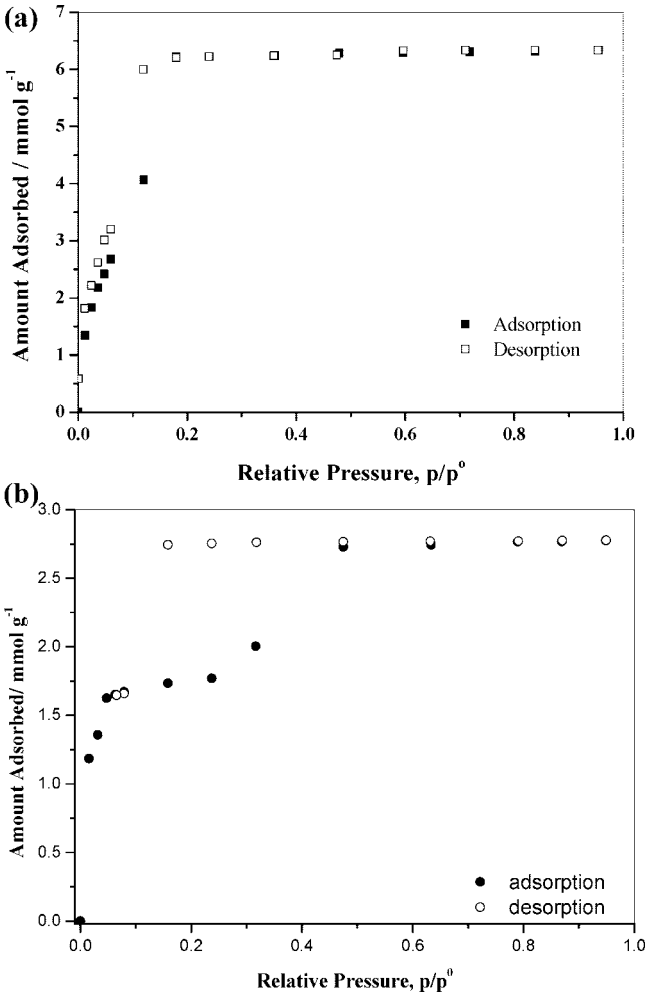

Figure 2. Adsorption isotherms for M′MOF **1** ($Zn_3(BDC)_3Cu(Pyen)$) at 298 K (a) methanol (b) benzene.

Both the methanol (0.257 $cm^3\ g^{-1}$) and benzene (0.248 $cm^3\ g^{-1}$) pore volumes are significantly lower than the crystallographic pore volume obtained using PLATON (0.286 $cm^3\ g^{-1}$). The molecular dimensions, obtained from ZINDO calculations, for benzene[81] are 3.277 × 6.628 × 7.337 Å and for methanol[82,83] are 3.81 × 4.18 × 4.95 Å. Comparison of these dimensions with the pore dimensions of M′MOF **1** indicate that part of the irregular ultramicropores in the direction of the *b* crystallographic axis may not be accessible to these molecules. In contrast, the curved pores of about 5.6 × 12.0 Å in the direction of the *c* crystallographic axis are accessible to both benzene and methanol molecules.

3.3. H_2 and D_2 Adsorption Isotherms. Figure 3 shows the adsorption isotherms for purified H_2 and D_2 on M′MOF **1**. The isotherms are type I in the IUPAC Classification scheme.[13] The isotherms only show a very small amount of hysteresis (see Supporting Information). The standard deviations for the repeatability of the amounts adsorbed (*n*) for isotherm points averaged ±0.66% and ±0.64% for adsorption of H_2 and D_2 over the pressure (*p*) range 0.5–100 kPa at 77.3 K (see Supporting Information). The corresponding values for H_2 adsorption at

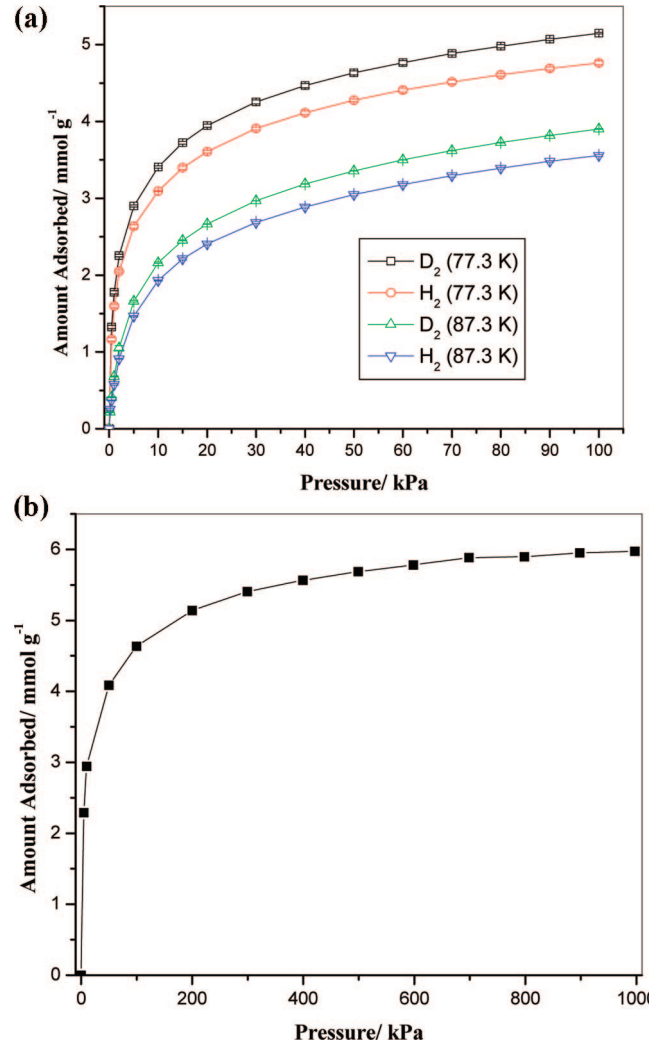

Figure 3. Isotherms for H_2 and D_2 adsorption on M′MOF **1** ($Zn_3(BDC)_3Cu$-(Pyen)): (a) Pressure range 0−1 bar at 77.3 and 87.3 K. (b) Pressure range 0−1 MPa for H_2 at 77.3 K.

87.3 K were ±0.63 and ±0.51%, respectively. The largest errors for isotherm points were at low pressure (0.5–1 kPa) and these were ∼1.55% and 1.49% for H_2 adsorption at 77.3 and 87.3 K, respectively. The corresponding values for D_2 were ∼1.71% and 1.10% for adsorption at 77.3 and 87.3 K, respectively. These isotherm repeatability values are similar to those obtained for carbon molecular sieve CMS T3A.[70]

Comparison of the molar D_2/H_2 ratios (nD_2/nH_2) for specific adsorption points at 77.3 K showed that they did not change markedly with pressure in the range 0.5–100 kPa (see Figure 4 and Supporting Information) and averaged 1.094 ± 0.016 at 77.3 K and 1.114 ± 0.023 at 87.3 K. The former value is similar to the average nD_2/nH_2 ratio for specific isotherm points for carbons G212 (1.076 ± 0.006),[84] CMS T3A (1.063 ± 0.004), carbon PCS (1.097 ± 0.009) for 0.5–100 kPa,[70] and carbon nanohorns gave values 1.06−1.08.[85] Similar values of 6–9% greater D_2 than H_2 adsorption at 77.3 K were reported for graphitised carbon blacks and activated carbons[84,86,87] The

(81) Webster, C. E.; Drago, R. S.; Zerner, M. C. *J. Am. Chem. Soc.* **1998**, *120*, 5509–5516.
(82) Fletcher, A. J.; Thomas, K. M. *Langmuir* **2000**, *16*, 6253–6266.
(83) Webster, C. E. Calculations carried out by the methods in ref 81 and reported as a private communication in reference 82.
(84) Zhao, X. B.; Xiao, B.; Fletcher, A. J.; Thomas, K. M. *J. Phys. Chem. B* **2005**, *109*, 8880–8888.
(85) Tanaka, H.; Kanoh, H.; Yudasaka, M.; Iijima, S.; Kaneko, K. *J. Am. Chem. Soc.* **2005**, *127*, 7511–7516.
(86) Yaris, R.; Sams, J. R. J. *J. Chem. Phys.* **1962**, *37*, 571–576.

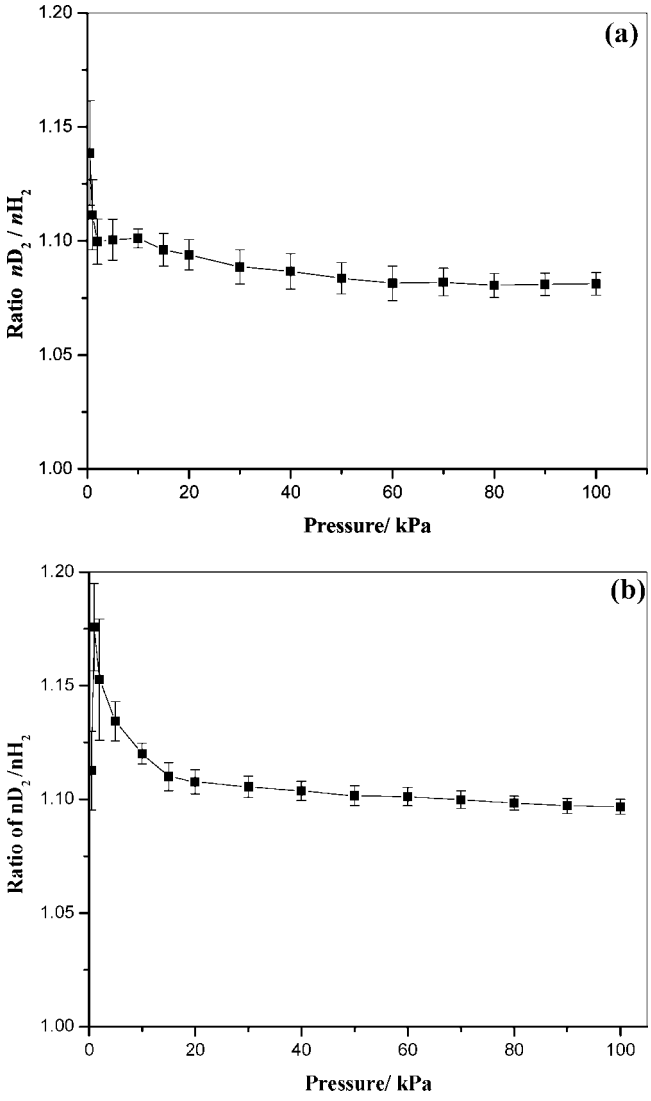

Figure 4. Variation of nD_2/nH_2 with amount adsorbed for adsorption on M′MOF **1** ($Zn_3(BDC)_3Cu(Pyen)$) at (a) 77.3 and (b) 87.3 K.

adsorption of D_2 on charcoal over the temperature range 55–90 K was 8% greater than that of H_2, whereas in the range 17–20 K, the D_2 adsorption was 15% greater.[87] These results for nD_2/nH_2 ratios show that quantum effects influence the adsorption isotherms. The de Broglie wavelength becomes longer with decreasing temperature and therefore, the difference between D_2 and H_2 adsorption is expected to increase with decreasing temperature. The average nD_2/nH_2 ratio in this study is slightly higher at 87.3 K than 77.3 K with the difference being <1 standard deviation (σ) and, therefore, within the experimental uncertainty of the measurements.

Metal−organic frameworks gave values in the range 1.05–1.20 for the molar ratio of adsorbed D_2/H_2 over the pressure range 1–90 kPa for $Cu_2((O_2C)_2–C_6H_3–C_6H_4–C_6H_3–(CO_2)_2)$[59] and 1.144 ± 0.057 for pressure range 0.5–80 kPa for HKUST-1.[88] A nD_2/nH_2 ratio of 1.16 was observed for adsorption on zeolite NaA at 77.3 K.[89] The desorption isotherms for the carbons showed similar trends for the nD_2/nH_2 ratios to those obtained for adsorption.[70] It is evident that the nD_2/nH_2 ratios are similar for adsorption on a wide variety of porous structures at 77.3 K.

The maximum amount of hydrogen adsorbed was calculated using the Langmuir equation which can be expressed in the following form:[19]

$$p/n = 1/n_m b + p/n_m \quad (2)$$

where p is the pressure, n the amount adsorbed, n_m is the monolayer capacity and b is the coefficient of adsorption specific to the adsorbate/adsorbent system. Analysis of the isotherm data in Figure 3b showed that the Langmuir graph was slightly curved. Analysis of data for the pressure range 500–1000 kPa using eq 2 gave a maximum amount adsorbed of 6.72 mmol g^{-1} (1.35 wt %) while data for the pressure range 100–1000 kPa gave a value of 6.21 mmol g^{-1} (1.25 wt %). Therefore, the maximum amount of H_2 adsorbed is in the range 6.21–6.72 mmol g^{-1}. The densities of adsorbed hydrogen calculated using the maximum amount of H_2 adsorbed (6.72 mmol g^{-1}) and methanol pore volume (0.257 cm^3 g^{-1}), benzene pore volume (0.248 cm^3 g^{-1}) and Platon pore volume (0.286 cm^3 g^{-1}) were 0.0546, 0.0527 and 0.0473 g cm^{-3}, respectively. The ranges are similar to adsorbed hydrogen density values obtained previously.[59,70,84,88] However, the density of liquid H_2 is 0.0708 g cm^{-3} (35.12 mol L^{-1}) at 20.2 K.[78] The liquid densities of hydrogen isotopes vary significantly with temperature. D_2 has a higher density (41.9 mol L^{-1} at 22.24 K[78]) than H_2 on a mole basis at a similar temperature. Therefore, the higher amount of D_2 adsorbed compared with H_2 is consistent with the higher density of liquid D_2. This is related to the lower zero-point energy for D_2.

3.4. Virial Graphs. Isotherm data were analyzed using the virial equation:[70,84,90–94]

$$\ln(n/p) = A_0 + A_1 n + A_2 n^2 .... \quad (3)$$

where p is pressure, n is amount adsorbed and A_0, A_1 etc. are virial coefficients. A_0 is related to adsorbate–adsorbent interactions, whereas A_1 describes adsorbate–adsorbate interactions. The Henry's Law constant (K_H) is equal to $\exp(A_0)$. The virial graphs for H_2 and D_2 adsorption on M′MOF **1** at 77.3 and 87.3 K are shown in Figure 5, and the virial parameters are given in Table 1. The graphs are linear for the pressure ranges 0.5–30 kPa (0–4 mmol g^{-1} and 0–4 H_2 molecules per $Zn_3(BDC)_3Cu$-(Pyen) formula unit) and 0.5–10 kPa (∼0–2 mmol g^{-1} and 0–2 H_2 molecules per $Zn_3(BDC)_3Cu(Pyen)$ formula unit) for adsorption at 77.3 and 87.3 K, respectively. Virial graphs for H_2 adsorption on a wide range of porous carbons at 77.3 K are also linear over a relatively large surface coverage range. The virial graphs for both H_2 and D_2 adsorption on M′MOF **1** at 87.3 K deviate from linearity and have two linear regions. The point where the gradient in the virial graphs changes corresponds

(87) van Dingenen, W.; van Itterbeek; A. *Physica (The Hague)* **1939**, *6*, 49–58.
(88) Xiao, B.; Wheatley, P. S.; Zhao, X.; Fletcher, A. J.; Fox, S.; Rossi, A. G.; Megson, I. L.; Bordiga, S.; Regli, L.; Thomas, K. M.; Morris, R. E. *J. Am. Chem. Soc.* **2007**, *129*, 1203–1209.
(89) Stephanie-Victoire, F.; Goulay, A. M.; de Lara, E. C. *Langmuir* **1998**, *14*, 7255–7259.
(90) Cole, J. H.; Everett, D. H.; Marshall, C. T.; Paniego, A. R.; Powl, J. C.; Rodriguez-Reinoso, F. *J. Chem. Soc., Faraday Trans* **1974**, *70*, 2154–2169.
(91) O'koye; I. P.; Benham, M.; Thomas, K. M. *Langmuir* **1997**, *13*, 4054–4059.
(92) Reid, C. R.; O'koye, I. P.; Thomas, K. M. *Langmuir* **1998**, *14*, 2415–2425.
(93) Reid, C. R.; Thomas, K. M. *Langmuir* **1999**, *15*, 3206–3218.
(94) Reid, C. R.; Thomas, K. M. *J. Phys. Chem. B* **2001**, *105*, 10619–10629.

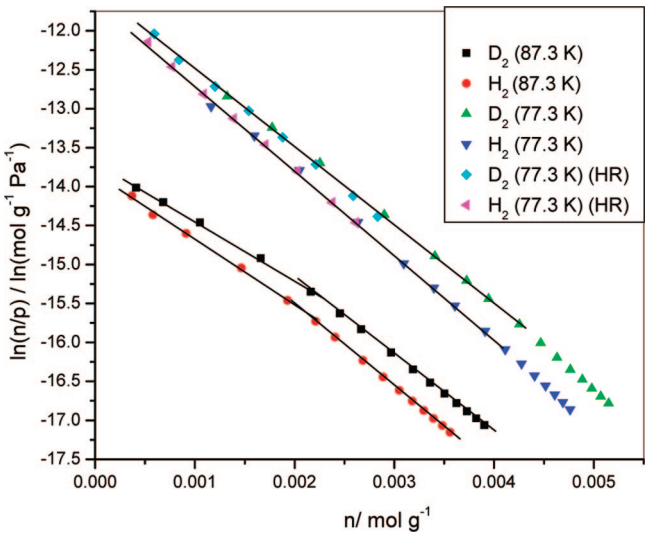

Figure 5. Virial graphs for H_2 and D_2 adsorption on M′MOF **1** ($Zn_3(BDC)_3$-Cu(Pyen)) at 77.3 and 87.3 K. (HR = High Resolution).

to two H_2 (or D_2) molecules per open Cu center (~1.92 mmol g^{-1}). This is consistent with four-coordinate Cu centers increasing to six-coordinate by adsorption of two H_2 molecules either side of the CuN_2O_2 plane. The virial parameters A_1 were determined from the data for 0.5–10 kPa data (n = <2 mmol g^{-1}). The virial graphs for H_2 and D_2 adsorption at 87.3 K, above 2 mol g^{-1} amount adsorbed, were also linear and the gradients were 1054 ± 1.5 g mol^{-1} (R^2 = 0.99998) and 988.3 ± 2.2 g mol^{-1} (R^2 = 0.99996). These values are very similar to the corresponding A_1 values at 77.3 K, shown in Table 1. This change in gradient occurs at adsorption of 2 H_2 per Cu in the formula unit. Therefore, it is attributed to changes in surface chemistry.

Virial parameters A_0 and A_1 are less negative for D_2 than for the corresponding H_2 adsorption at both 77.3 and 87.3 K. The A_0 values indicate that K_H is higher for D_2, indicating slightly stronger adsorbate–adsorbent interactions for D_2. This is attributed to competing quantum effects: 1) the quantum statistical mass effect on the vibrational energy levels normal to the surface and 2) the quantum mechanical effect of isotopic substitution on the dispersion energy.[86] The values of A_1 for H_2 and D_2 obtained at 77.3 K are similar to those obtained previously for H_2 and D_2 adsorption on carbons at 77.3 K[70] and also similar to those obtained for adsorption of a range of gases (nitrogen, carbon dioxide etc.) on a carbon molecular sieve over the temperature range 303–343 K.[91–94] The A_1 values for D_2 adsorption are ~7–8 standard deviations (σ) lower than for H_2 adsorption for M′MOF **1**, and this difference is similar to carbon molecular sieve CMS T3A and porous carbon PCS.[70] The differences in A_1 are statistically significant, indicating higher repulsion energies between neighbors for H_2 than for D_2. This is related to the larger zero-point energy of H_2 compared with that of D_2.

3.5. Variation of Hydrogen Adsorption as a Function of Temperature. The change in the integral heat of adsorption Q with respect to temperature is described by the following equation:

$$\frac{dQ}{dT} = n_s(Cp_G - Cp_S) \quad (4)$$

where n_s is the amount adsorbed, Cp_G is the molar heat capacity of the gas phase at constant pressure, Cp_S is the molar heat capacity of the adsorbed phase and T is the temperature.[95] At zero surface coverage the enthalpy of adsorption is constant. This was used as a test for the accuracy of the isotherm measurement protocols.[84] The isosteric enthalpies of adsorption ($Q_{st,n=0}$) at zero surface coverage were calculated from the A_0 virial parameters determined using eq 3 for adsorption data at 77.3 and 87.3 K. The values for H_2 and D_2 were 12.29 ± 0.53 and 12.44 ± 0.50 kJ mol^{-1}, respectively. Previous results for the enthalpy of adsorption of H_2 on MOFs and other porous materials are given in Table 2. The enthalpy of adsorption of H_2 on M′MOF **1** is the highest reported so far. The $Q_{st,n=0}$ value for D_2 at zero surface coverage is slightly higher than for H_2 but this is not statistically significant. This is consistent with higher K_H values for D_2 compared with H_2 adsorption and nD_2/nH_2 ratios >1 (see section 3.3). Studies of H_2 and D_2 adsorption on carbon also showed that the enthalpy of adsorption was 0.75 kJ mol^{-1} higher for D_2 adsorption.[87]

Calculations of the isosteric enthalpies of adsorption at specific surface coverage require accurate interpolation between isotherm points to obtain pressures for specific surface coverages for isotherms obtained at various temperatures and this requires the use of isotherm models. The most appropriate model to use depends on the shape of the isotherm. The models that can be used are limited because H_2 and D_2 adsorption at 77 K are above the critical temperatures and saturated vapor pressures do not exist under supercritical conditions.

The ln(p) values for given amount adsorbed were calculated from the linear regressions determined from the virial equation analysis using eq 3 described above. In the case of H_2 and D_2 adsorption at 87.3 K, the equations for the two linear regions (see Figure 5) were used for calculating ln(p) values. The isotherm data used for calculating the graphs of isosteric enthalpy of adsorption for H_2 and D_2 adsorption on M′MOF **1** had an average standard deviation (σ) of ±0.63% while the values calculated using the method described above gave ±0.52% (see Supporting Information). It is evident that the model provides an accurate description of the isotherm since the average deviation of the model from the experimental data for the four isotherms was <1 σ. The enthalpies of adsorption of H_2 and D_2 for specific surface coverages were calculated using the van't Hoff isochore and the results are shown in Figure 6. It is evident that the enthalpy of adsorption decreases with increasing amount adsorbed up to n = ~1.9 mmol g^{-1} (two H_2 molecules per open Cu site). Figure 6 shows that in the amount adsorbed range 2–3.6 mmol g^{-1} (>50% surface coverage) the enthalpy of adsorption is virtually unchanged and was high (9.5 kJ mol^{-1}) for both H_2 and D_2 adsorption. The enthalpies of adsorption for H_2 were slightly lower than for D_2 at low surface coverage although this is within experimental error and the trend is expected for nD_2/nH_2 >1.

Rowsell *et al.*[96] used an alternative virial method based on the following equation:[97–99]

$$\ln(p) = \ln(n) + (1/T)\sum_{i=0}^{m} a_i n^i + \sum_{j=0}^{n} b_j n^j \quad (5)$$

(95) Cerny, S. *Chem. Phys. Solid Surf. Heterog. Catal.* **1983**, *2*, 1–57.
(96) Rowsell, J. L. C.; Yaghi, O. M. *J. Am. Chem. Soc.* **2006**, *28*, 1304–1315.
(97) Czepirski, L.; Jagiello, J. *Chem. Eng. Sci.* **1989**, *44*, 797–801.
(98) Jagiello, J.; Bandosz, T. J.; Schwarz, J. A. *Langmuir* **1996**, *12*, 2837–2842.
(99) Anson, A.; Jagiello, J.; Parra, J. B.; Sanjuan, M. L.; Benito, A. M.; Maser, W. K.; Martinez, M. T. *J. Phys. Chem. B* **2004**, *108*, 15820–15826.

Table 1. Comparison of Virial Parameters for Adsorption of H_2 and D_2 on M′MOF **1** ($Zn_3(BDC)_3Cu(Pyen)$) at 77.3 and 87.3 K, and Carbon Molecular Sieve CMS T3A and Carbon PCS at 77.3 K[b]

	T/K	adsorbate	run	K_H/mol g^{-1} Pa^{-1}	A_0/ln (mol g^{-1}Pa^{-1})	A_1/g mol^{-1}	P range/kPa
CMS T3A[70]	77	H_2		1.206×10^{-5}	-11.326 ± 0.034	-1063.9 ± 9.4	
		D_2		1.243×10^{-5}	-11.295 ± 0.032	-992.4 ± 8.3	
PCS[70]	77	H_2		7.075×10^{-6}	-11.859 ± 0.035	-962.5 ± 12.0	
		D_2		7.795×10^{-6}	-11.762 ± 0.015	-879.0 ± 10.0	
M′MOF **1**[a]	77	H_2	1	8.335×10^{-6}	-11.695 ± 0.043	-1065.9 ± 15.1	0.5–30 (<4 mmol g^{-1})
			2	8.495×10^{-6}	-11.676 ± 0.059	-1057.5 ± 20.7	
			3	9.030×10^{-6}	-11.615 ± 0.032	-1084.6 ± 11.4	
			average isotherm	8.615×10^{-6}	-11.662 ± 0.044	-1069.1 ± 15.8	
		D_2	1	1.051×10^{-5}	-11.463 ± 0.032	-1000.4 ± 10.9	0.5–20 (<4 mmol g^{-1})
			2	9.860×10^{-6}	-11.527 ± 0.037	-993.0 ± 12.8	
			3	1.069×10^{-5}	-11.446 ± 0.029	-1005.7 ± 10.0	
			average isotherm	1.033×10^{-5}	-11.480 ± 0.032	-999.4 ± 11.0	
M′MOF **1**[a]	87	H_2	1	9.739×10^{-7}	-13.842 ± 0.020	-827.3 ± 16.9	0.5–10 (<2 mmol g^{-1})
			2	9.827×10^{-7}	-13.833 ± 0.022	-842.2 ± 18.8	
			3	9.709×10^{-7}	-13.845 ± 0.046	-837.2 ± 38.8	
			average isotherm	9.768×10^{-7}	-13.839 ± 0.028	-835.9 ± 23.5	
		D_2	1	1.168×10^{-6}	-13.660 ± 0.047	-762.5 ± 34.1	0.5–10 (<2 mmol g^{-1})
			2	1.106×10^{-6}	-13.715 ± 0.015	-744.5 ± 11.0	
			3	1.152×10^{-6}	-13.674 ± 0.026	-768.3 ± 19.1	
			average isotherm	1.143×10^{-6}	-13.682 ± 0.024	-759.1 ± 17.8	

[a] Errors for individual isotherms were obtained from the corresponding virial graphs. [b] Average Isotherm is the average of isotherms 1, 2, and 3. Errors quoted are those obtained from the corresponding virial graph.

Table 2. Literature Values for Isosteric Enthalpies of Adsorption of H_2 on Metal−Organic Framework Materials

MOF	isosteric enthalpy of adsorption Q_{st}/kJ mol^{-1}	temp range/K	ref
PCN-9	10.1	77–87	116
MOF-5	5.2	77–195	96
prussian blue	5.3–7.4	77–87	105
MOF-74	8.3	77–195	96
HKUST-1	6.6		96
IRMOF-11	5.1–9.1		96
MgMOF long	7–9.5	77–87	39
ion-exchanged variants of $Mn_3[(Mn_4Cl)_3$-$(BTT)_8(CH_3OH)_{10}]_2$	10.5	77–87	66
functionalizedcarbons	3.9–5.2	77–114	84
carbons	1.4–7.3, 6–7.9	17–90, 77–90	87, 117
zeolite Na-A	6.2–10.7	40–120	89
zeolites 4A, 5A, 13X	5.9–7.9	75–90	117
silica gel	5.4–7.3	75–90	117
$NaNi_3(OH)(SIP)_2$	9.4–10.4	77–87	102

where p is pressure, n is amount adsorbed, T is temperature, and a_i and b_j are temperature independent empirical parameters. The isosteric enthalpy of adsorption (Q_{st}) is obtained from the following equation:

$$Q_{st} = -R\sum_{i=0}^{m} a_i n^i \qquad (6)$$

where R is the gas constant. The isotherm data for H_2 and D_2 adsorption at 77.3 and 87.3 K were fitted to this with unit weights. The isosteric enthalpies calculated as a function of surface coverage are compared with those calculated by the other methods in Supporting Information. Good agreement was obtained between the virial methods for H_2 and D_2 adsorption on M′MOF **1**, but this nonparametric regression method was more complicated to use than the simpler virial equation based on equation 3. Also, the fitting of the model was not quite as good as the virial method based on equation 3 since values calculated using this method gave an average deviation ±0.69% (see Supporting Information). The enthalpies of adsorption for H_2 were slightly higher than those for D_2 but this is within the experimental uncertainty in the measurements and opposite to the trend expected from nD_2/nH_2 ratios.

An alternative approach involves the use of the Langmuir−Freundlich equation:

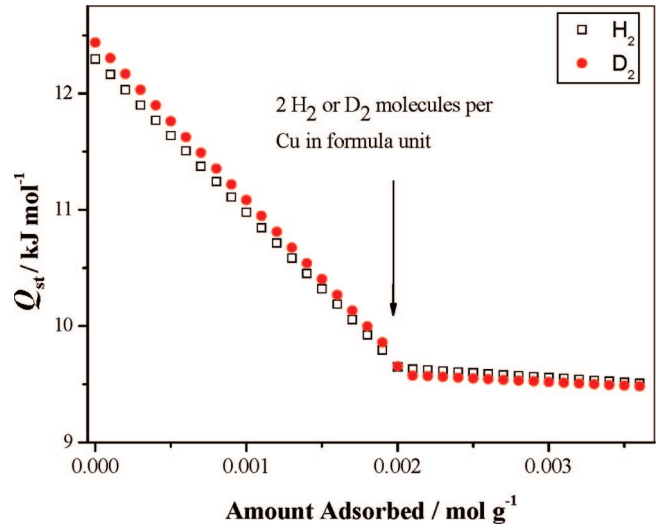

Figure 6. Variation of isosteric enthalpy of adsorption (Q_{st}/kJ mol^{-1}) with amount adsorbed (mol g^{-1}) for H_2 and D_2 adsorption on M′MOF **1** ($Zn_3(BDC)_3Cu(Pyen)$).

$$\left(\frac{n}{n_L}\right) = \left(\frac{kp^{1/m}}{1 + kp^{1/m}}\right) \qquad (7)$$

where n is the amount adsorbed, n_L is the limiting amount adsorbed, p is the pressure and k and m are constants. Comparison of fitting isotherms based on this model and the isotherm data are shown in Supporting Information. The greatest uncertainties in the interpolations are in the low pressure region where the isotherm is steepest. The reason for this is that the Langmuir−Freundlich equation does not reduce to Henry's Law at low surface coverage. Q_{st} values were calculated using a modification of the Clausius–Clapeyron equation. The isosteric enthalpy values at low surface coverage are slightly higher than the values obtained using both virial equation methods. However, the shape of the enthalpy versus amount adsorbed graph is similar to those obtained by virial methods and good agreement was obtained for uptakes $\gtrsim$1.5 mmol g^{-1} (see Supporting Information).

Virial method 1 based on equation 3 is preferred because the linearity in the low pressure part of the isotherm provides

direct confirmation of the accuracy of the interpolations. Also, the intercept of the graph gives A_0, where the Henry's Law constant $K_H = \exp(A_0)$ and this is a measure of the H_2 surface interaction. Comparison of the three models with the uncertainties determined for the experimental isotherm data showed that virial method 1 based on equation 3 provided the most accurate description of the H_2 and D_2 isotherms for M′MOF **1** with agreement averaging <1 standard deviation.

Evidence for molecular chemisorptions has been obtained from inelastic neutron scattering studies for H_2 adsorption on Fe-ZSM-5,[100] Cu exchanged ZSM-5 zeolite,[101] porous nickel phosphate VSB-5[65] and porous hybrid inorganic/organic framework material $NaNi_3(OH)(SIP)_2$ where SIP = 5-sulfoisophthalate.[102] Other studies of unsaturated metal centers in metal−cyano[103–106] and metal−organic framework materials have suggested that the H_2 interactions in these materials are much weaker.[64,104,107] The high hydrogen uptakes did not relate to the presence of metal centers. This is presumably due to the small proportion of the surface represented by the metal centers. The high enthalpies of adsorption for H_2 and D_2 adsorption on M′MOF **1** are a minimum of ~9.5 kJ mol^{-1} at 3.6 mmol g^{-1} H_2 or D_2 uptake, which is well above the saturation limit of 2 molecules per unsaturated metal center. The above trends in enthalpies of adsorption for M′MOF **1** are consistent with surface chemistry and pore confinement enhancing the isosteric enthalpy of adsorption. It is possible that the decrease in enthalpy of adsorption from 12.3 to 9.5 kJ mol^{-1} for 0−1.9 mmol g^{-1} H_2 or D_2 uptake reflects strong adsorption on open Cu sites either side of the CuN_2O_2 plane when confined in very narrow pores. Inelastic neutron scattering and FTIR studies are underway of H_2 adsorption on M′MOF **1** at low surface coverage to establish if a strong interaction occurs between H_2 and unsaturated metal centers.

3.6. H_2 and D_2 Adsorption and Desorption Kinetics. The double exponential (DE) model is described by the following equation.

$$\frac{M_t}{M_e} = A_1(1 - e^{-k_1 t}) + (1 - A_1)(1 - e^{-k_2 t}) \qquad (8)$$

where M_t is the uptake at time t, M_e is the equilibrium uptake, k_1 and k_2 are the rate constants and A_1 and $(1 - A_1)$ are the fractional contributions for process mechanisms corresponding to adsorption rate constants k_1 and k_2, respectively. This model describes two kinetic processes each with different relaxation times. Diffusion of ethanol and methanol into $Ni_2(4,4'\text{bipyridine})_3(NO_3)_4$ porous framework materials templated with ethanol (E) and methanol (M) followed the DE model.[10,11] Since there are equal numbers of pore cavities and windows in these materials, as shown from crystallographic studies, diffusion through both structural features have equal contributions (A_1 = 0.5). The kinetics can be described by two processes with single relaxation times, (a) slow diffusion through windows with high activation energy and (b) fast diffusion along pore cavities with low activation energy.

M′MOF **1** has two types of pores and diffusion along these pores have different kinetic characteristics. Parts a and b of Figure 7 show adsorption profiles for a typical isotherm pressure increment for both H_2 and D_2 at 77.3 and 87.3 K. The rates of adsorption of D_2 are faster than the corresponding profiles for H_2 and the rates of adsorption increase with increasing amount adsorbed (See Figure 8). The kinetic profiles can be described by a double exponential (DE) model and typical comparisons of normalized experimental and calculated profiles are shown in Figure 7. It is evident that the DE model provides a good description of the adsorption kinetics. The slow rate constant (k_1) corresponds to diffusion along the narrowest pores in the direction of the crystallographic b axis direction and the fast rate constant (k_2) corresponds to diffusion in the c axis direction through larger pores with size 5.6 × 12.0 Å. The repeatability of the individual kinetic rate constants, k_1 and k_2 obtained from the DE kinetic model for H_2 and D_2 adsorption were determined. The average errors for k_1 and k_2 for H_2 adsorption, over the pressure range 2–10 kPa at 87.3 K and 0.1–5 kPa at 77.3 K were ±4.1 and ±3.5%, respectively. The corresponding average errors for k_1 and k_2 for D_2 adsorption were ±3.2 and 2.9%, respectively. The ratio of rate constants (k_2/k_1) for various pressure increments decreases with increasing pressure over the ranges 6.64–3.48 and 5.88–2.96 for H_2 and D_2 adsorption at 77.3 K. At 87.3 K, the corresponding ranges for k_2/k_1 ratios for H_2 and D_2 adsorption were 3.24–2.05 and 3.02–1.98, respectively. The lower values for the ratios at 87.3 K indicate the strong effect of temperature on quantum effects which give rise to barriers to diffusion of H_2 and D_2 into the porous structure.

Figure 8 shows that the kinetic parameters $\ln(k_1)$ and $\ln(k_2)$ have a linear variation with amount adsorbed. The kinetic data for the normal isotherm resolution at 77.3 K showed that there was only limited kinetic data at low surface coverage compared with the isotherm data for 87.3 K, which had lower amounts adsorbed. Therefore, isotherm studies were repeated at higher resolution in the low pressure region for H_2 and D_2 adsorption at 77.3 K in order to determine the kinetic parameters at low surface coverage so that kinetic parameters could be obtained in the same detail over the same H_2 uptake ranges. This allowed extrapolations to determine the kinetic parameters at zero surface coverage ($\ln(k_{1,n=0})$ and $\ln(k_{2,n=0})$) and values of $\ln(k_1)$ and $\ln(k_2)$ at specific surface coverages to be obtained with greater precision. The virial graphs for the high resolution isotherm (0.1–5 kPa) data gave A_0 and A_1 parameters (see Supporting Information) that were identical within experimental error to those obtained for data (0.5–30 kPa) from the other isotherms (see Table 1).

3.7. Comparison of H_2 and D_2 Adsorption/Desorption Characteristics. The average ratios of rate constants kD_2/kH_2 for the slow component (k_1) were 1.62 ± 0.07, while values for the fast component (k_2) were 1.38 ± 0.04 for M′MOF **1** at 77.3 K. The corresponding ratios for the slow and fast adsorption kinetic components at 87.3 K were 1.32 ± 0.09 and 1.21 ± 0.05 for k_1 and k_2, respectively. It is evident that the ratio is higher for the slower rate constant, corresponding to diffusion along the narrowest pores in the direction of the b axis, than for the pores in the direction of the c axis. Also, temperature

(100) Mojet, B. L.; Eckert, J.; Santen, R. A. v.; Albinati, A.; Lechner, R. E. *J. Am. Chem. Soc.* **2001**, *123*, 8147–8148.
(101) Georgiev, P. A.; Albinati, A.; Mojet, B. L.; Ollivier, J.; Eckert, J. *J. Am. Chem. Soc.* **2007**, *129*, 8086–8087.
(102) Forster, P. M.; Eckert, J.; Heiken, B. D.; Parise, J. B.; Yoon, J. W.; Jhung, S. H.; Chang, J. S.; Cheetham, A. K. *J. Am. Chem. Soc.* **2006**, *128*, 16846–16850.
(103) Chapman, K. W.; Southon, P. D.; Weeks, C. L.; Kepert, C. J. *Chem. Commun.* **2005**, *26*, 3322–3324.
(104) Chapman, K. W.; Chupas, P. J.; Maxey, E. R.; Richardson, J. W. *Chem. Commun.* **2006**, *38*, 4013–4015.
(105) Kaye, S. S.; Long, J. R. *J. Am. Chem. Soc.* **2005**, *127*, 6506–6507.
(106) Prestipino, C.; Regli, L.; Vitillo, J. G.; Bonino, F.; Damin, A.; Lamberti, C.; Zecchina, A.; Solari, P. L.; Kongshaug, K. O.; Bordiga, S. *Chem. Mater.* **2006**, *18*, 1337–1346.
(107) Hartman, M. R.; Peterson, V. K.; Liu, Y.; Kaye, S. S.; Long, J. R. *Chem. Mater.* **2006**, *18*, 3221–3224.

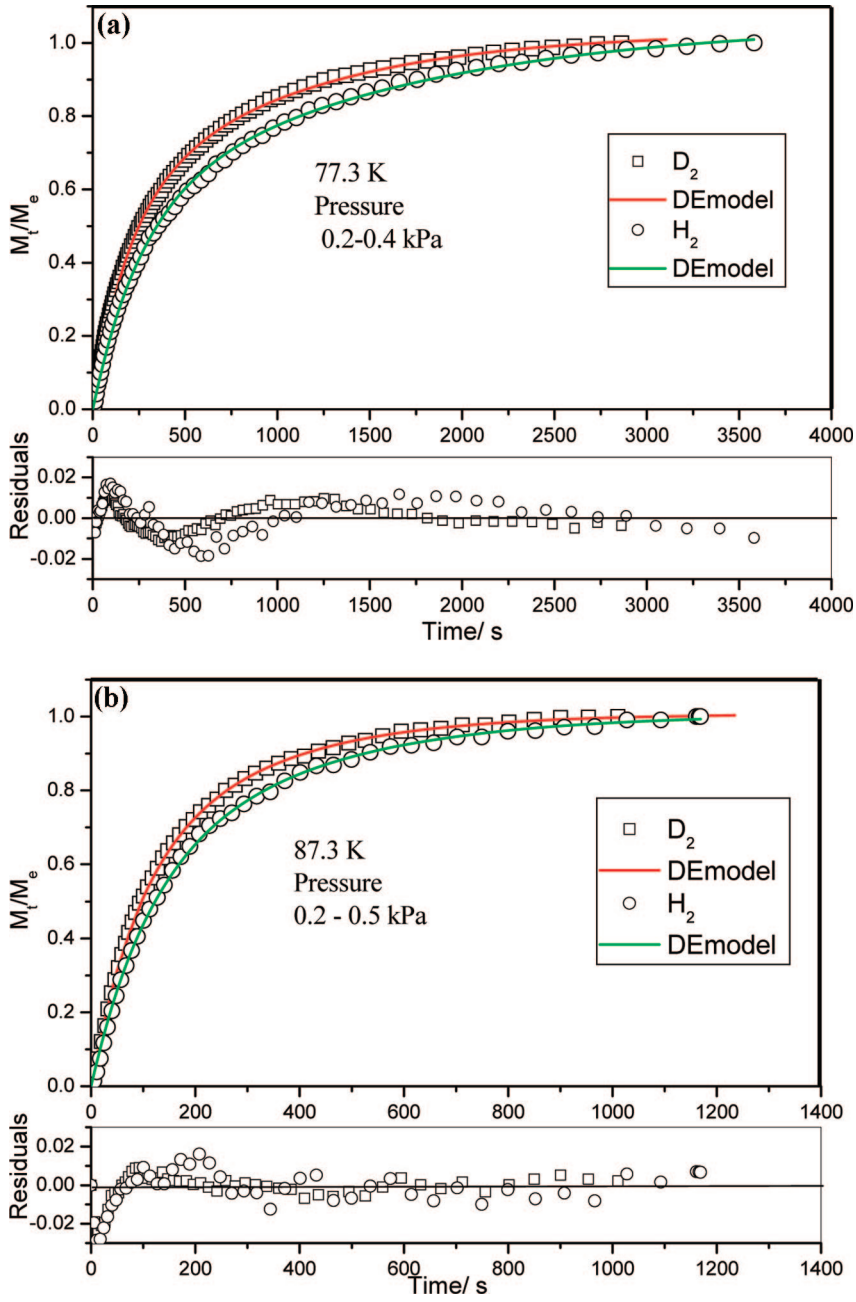

Figure 7. Comparison of H_2 and D_2 kinetic profiles and the corresponding fit for DE kinetic model with residuals for adsorption on M′MOF **1** ($Zn_3(BDC)_3Cu(Pyen)$): (a) Pressure increment 0.2–0.4 kPa at 77.3 K; (b) pressure increment 0.2–0.5 kPa at 87.3 K.

has a large effect on the kD_2/kH_2 ratio. Previous studies of a carbon molecular sieve (CMS T3A) with kinetic selectivity, incorporated by carbon deposition, and carbon (PCS), similar to the CMS T3A substrate showed that narrowing the porosity by carbon deposition increased kD_2/kH_2 from 1.35 to 1.9.

Nitrogen adsorption was investigated in detail for these carbons, and the activation energies for diffusion at zero surface coverage were determined. The activation energy for adsorption of nitrogen on CMS T3A was much higher (32.33 ± 0.26 kJ mol^{-1}: temperature range 273–323 K) compared with PCS (6.02 ± 0.94 kJ mol^{-1}: temperature range 262–276 K). The same order for the kinetic barriers for H_2 and D_2 adsorption is expected. The kinetic barrier is much higher in CMS T3A, and this corresponds to diffusion through kinetically selective carbon deposit material, which gives slower rate constants for CMS T3A than for PCS for the same pressure increments and higher ratios of kD_2/kH_2, indicating a relationship between the kinetic barriers and the isotope kinetic selectivity.

The DE rate constants k_1 and k_2 increase with increasing amount adsorbed. Therefore, the kinetic barriers to diffusion into the porous structure were calculated from the kinetic parameters at zero surface coverage ($k_{1,n=0}$ and $k_{2,n=0}$) and as a function of amount adsorbed. Measurements of the kinetic barriers for H_2 and D_2 adsorption on M′MOF **1** were determined from the rate constants $k_{1,n=0}$ and $k_{2,n=0}$ at zero surface coverage for adsorption at 77.3 and 87.3 K, and are given in Table 3. The barriers for the slow component (k_1) and the fast component (k_2) were 13.35 ± 0.59 and 8.56 ± 0.41 kJ mol^{-1} for H_2 adsorption on M′MOF **1**, respectively. The corresponding values for the slow and fast components for D_2 adsorption were 12.52 ± 0.47 and 8.04 ± 0.35 kJ mol^{-1}, respectively. The slow component has the higher barrier and the D_2 barriers for both

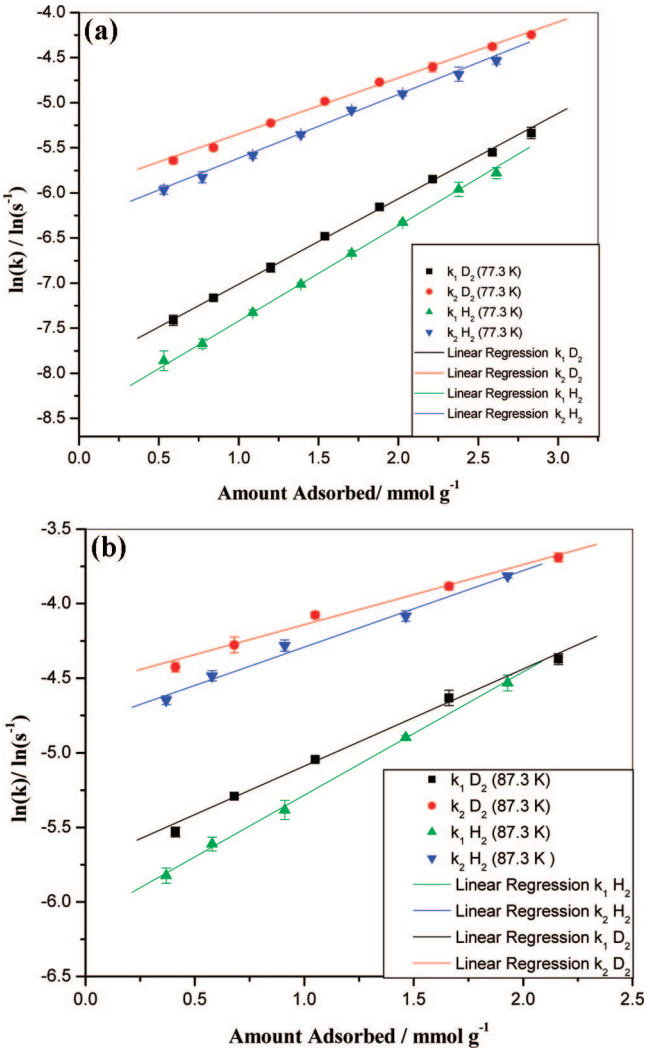

Figure 8. The variation of $\ln(k_1)$ and $\ln(k_2)$ obtained from the double exponential model with amount adsorbed for H_2 and D_2 adsorption on M′MOF **1** ($Zn_3(BDC)_3Cu(Pyen)$) at (a) 77.3 K and (b) 87.3 K.

Table 3. Kinetic Parameters at Zero Surface Coverage for H_2 and D_2 Adsorption on M′MOF **1** ($Zn_3(BDC)_3Cu(Pyen)$)[a]

gas	77.3 K	87.3 K	E_a/kJ mol^{-1}
	slow component, $\ln(k_{1,n=0})/\ln(s^{-1})$		
H_2	-8.475 ± 0.042	-6.111 ± 0.047	13.35 ± 0.59
D_2	-7.957 ± 0.015	-5.740 ± 0.023	12.52 ± 0.47
	fast component, $\ln(k_{2,n=0})/\ln(s^{-1})$		
H_2	-6.320 ± 0.042	-4.805 ± 0.027	8.56 ± 0.41
D_2	-5.966 ± 0.017	-4.542 ± 0.031	8.04 ± 0.35

[a] Temperature range 77.3–87.3 K.

components are slightly lower than the corresponding H_2 barriers although the difference is within the experimental uncertainty in the measurements. This is consistent with quantum effects due to the higher zero-point energy for H_2 compared with D_2, and smaller amplitude of vibration of the latter.

Figure 9 shows the variation of activation energy with amount adsorbed in the uptake range 0–2 mmol g^{-1} (0–2 H_2 per unsaturated metal center). It is evident that activation energies for both kinetic processes for both H_2 and D_2 decrease linearly with amount adsorbed. This is attributed to the influence of adsorbate–adsorbate interactions and the decrease in H_2 and D_2 surface interactions as shown by the decrease in enthalpies of adsorption with increasing amount adsorbed.

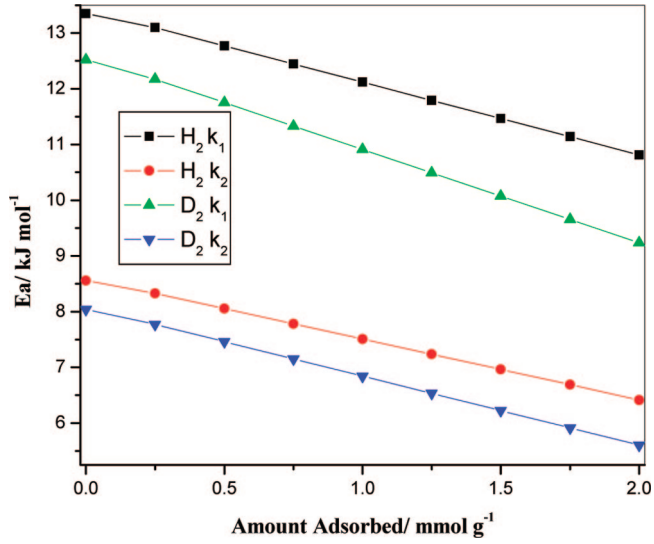

Figure 9. Variation of activation energy (E_a/kJ mol^{-1}) with amount adsorbed (mmol g^{-1}) for H_2 and D_2 adsorption on M′MOF **1** ($Zn_3(BDC)_3$-Cu(Pyen)).

3.8. Molecular Transport into Porous Materials. Diffusion of H_2 and D_2 into M′MOF **1** involves only surface diffusion since the pore sizes are much less than the mean free path. In the gas phase, both H_2 and D_2 have bond lengths of 0.7416 Å,[108] and therefore, differences in adsorption kinetics are not due to size. H_2 and D_2 have identical classical dimensions (2.40 × 2.40 × 3.14 Å) based on van der Waals radii and bond length. Small differences exist in the ortho and para spin isomer compositions with H_2 having 75% ortho form,[109] whereas D_2 has 67% at 77.3 K.[110] However, the isotherms and kinetic profiles at 77.3 and 87.3 K did not show any characteristics attributable to ortho and para forms of H_2 and D_2. Similar results have been observed for adsorption of H_2 and D_2 on carbon molecular sieves and porous carbons.[70] The de Broglie wavelengths for hydrogen and deuterium are ∼0.249 and 0.176 nm at 77.3 K, respectively. The radial degrees of freedom are restricted to one dimension for pores in the *b* axis direction and two dimensions, in 5.6 × 12.0 Å pores, in the *c* dimension. Quantum effects occur when the molecule and pore dimensions are similar. This barrier is greatest for the molecule with the highest zero-point energy. Therefore, while the sizes of H_2 and D_2 are the same, the barrier for diffusion through the pores is greatest for H_2 due to higher zero-point energy. Beenakker *et al.* predicted on the basis of a hard sphere/pore model, exclusion of H_2 from the porous structure due to the higher barrier related to the higher zero-point energy of H_2 compared with that of D_2.[68,69] Quantum isotope equilibrium effects with exclusion of H_2 were also predicted for adsorption on carbon nanotubes [111,112] and porous metal−organic framework materials.[113] This exclusion has not been observed in this study or for adsorption of H_2 and D_2 on carbons and other porous materials where nD_2/nH_2 ratios in the range 1.05–1.2 were observed.[59,70,84,88,89]

(108) Stoicheff, B. P. *Can. J. Phys* **1957**, *35*, 730–741.
(109) Giauque, W. F. *J. Am. Chem. Soc.* **1930**, *52*, 4816–4831.
(110) Johnston, H. L.; Long, E. A. *J. Chem. Phys.* **1934**, *2*, 389–395.
(111) Wang, Q.; Challa, S. R.; Sholl, D. S. J. K. J. *Phys. Rev. Lett.* **1999**, *82*, 956–959.
(112) Challa, S. R.; Sholl, D. S.; Johnson, J. K. *J. Chem. Phys.* **2002**, *116*, 814–824.
(113) Garberoglio, G.; Skoulidas, A. I.; Johnson, J. K. *J. Phys. Chem. B* **2005**, *109*, 13094–13103.

However, taking into consideration that the sizes of the isotopes are the same and the amplitudes of vibration of atoms, a sharp cutoff is not expected, and a region where kinetic effects are observed may be anticipated. This has been observed for adsorption on carbon molecular sieves and ultramicroporous carbon. The experimental work reported in this study demonstrates unequivocally that kinetic quantum molecular sieving for D_2 and H_2 occurs in M′MOF **1**.

Molecular simulation studies of diffusivity of H_2 and D_2 in zeolite **rho** pores indicated that the decreased well depth for H_2 led to the dominant effect being the increase in effective size parameter for the adsorbate–adsorbent interactions for H_2 compared with D_2.[114,115] The slower adsorption kinetics for H_2 compared with those of D_2 are attributed to diffusion through the two types of pores in the M′MOF **1** structure. It is interesting to note that isosteric enthalpies of adsorption (Figure 5) and activation energies (Figure 9) for both kinetic components are similar and have linear relationships, which decrease with increasing amount adsorbed (uptake range: 0–2 mmol g^{-1}). Therefore, linear correlations exist between the activation energies for both kinetic components and isosteric enthalpies for H_2 and D_2 adsorption on M′MOF **1**. The kinetic parameters k_1 and k_2 increase with increasing surface coverage, and $\ln(k_1)$ and $\ln(k_2)$ have linear relationships (Figure 8) with amount adsorbed (uptake range: 0–2.5 mmol g^{-1}). The results suggest that higher quantum molecular sieving is associated with a higher kinetic barrier and narrower selective porosity in the rate-determining diffusion into the porous structure. Furthermore, quantum effects have been observed for both types of pores in M′MOF **1**. The larger *c* pores have dimension 5.6 × 12.0 Å. Therefore, quantum effects are observed where 2-D diffusion may occur when the difference between the molecule and pore size, in one dimension, is similar to the de Broglie wavelength.

4. Conclusions

Mixed metal−organic framework $Zn_3(BDC)_3[Cu(Pyen)]\cdot(DMF)_5(H_2O)_5$ (M′MOF **1**) having 3^6 tessellated $Zn_3(BDC)_3$ 2-D sheets that are pillared by Cu(Pyen) to form a 3D structure, was synthesized, which on desolvation gives planar open copper centers. The structure has curved pores of about 5.6 × 12.0 Å in the *c* axis direction and irregular narrower ultramicropores in the direction of the *b* axis forming an approximately 2-D array of pores.

Virial analysis of the H_2 and D_2 isotherm data for M′MOF **1** indicated slightly greater D_2−surface than H_2−surface interactions, while D_2−D_2 interactions were lower than H_2−H_2 interactions. The former is attributed to differences in the quantum statistical mass effect on the vibrational energy levels normal to the surface and the dispersion energy, while the latter is attributed to the higher zero-point energy of H_2. The virial graphs at 87.3 K have a change in gradient at an uptake of $2H_2$ or D_2 per Cu, providing strong evidence for specific interactions.

There is an intrinsic difficulty in tuning pore surfaces to enhance H_2 physisorption interactions to compete with thermal energies. M′MOF **1** had the highest enthalpy of adsorption (12.3 kJ mol^{-1}), at zero surface coverage, thus far observed for adsorption of H_2. D_2 adsorption gave a slightly higher enthalpy of adsorption. The enthalpy of adsorption decreases with increasing amount adsorbed to ∼9.5 kJ mol^{-1} at 2 H_2 or D_2 per Cu (∼1.9 mmol g^{-1}). The enthalpies of adsorption were essentially constant in the range 1.9–3.6 mmol g^{-1}. Adsorption of H_2 and D_2 occurs on both sides of planar open Cu centers in ultramicroporosity and gives a very high enthalpy of adsorption over a wide range of surface coverage. A combination of open metal centers and confinement in pores, where potential energy fields overlap, enhances H_2−surface interactions.

The adsorption kinetics for H_2 and D_2 follow a double exponential model consistent with two different kinetic processes corresponding to diffusion along the two types of pores in M′MOF **1**. The rate constants for heavier D_2 were faster and the activation energies slightly lower than the corresponding values for H_2 kinetics for both components. This is attributed to quantum effects with the higher zero-point energy for H_2 giving a higher effective collision cross section than D_2, producing a higher barrier to diffusion along the pores. The differences between the sizes of H_2 or D_2 and the pores in M′MOF **1** are similar to the de Broglie wavelength in two dimensions (*b* axis direction pores) and one dimension (*c* axis direction pores). Two independent quantum effects for diffusion have been observed in the same material, a slower kinetic process for one-dimensional diffusion in very narrow porosity in the *b* axis direction and the other for pores (5.6 × 12.0 Å) in the *c* axis direction where two-dimensional diffusion occurs. Hence, only narrow porosity in one dimension is required for quantum effects to be observed. This is the first experimental observation of kinetic isotope quantum molecular sieving in MOF materials. This effect may have applications for isotope separation.

Acknowledgment. This work was supported by Leverhulme trust (KMT), an Award CHE 0718281 from the NSF (BC), and in part by the Welch Foundation Grant (BG-0017) to the Department of Chemistry at UTPA. This research was partially conducted at the Center for Nanophase Materials Sciences, which is sponsored at Oak Ridge National Laboratory by the Division of Scientific User Facilities, U.S. Department of Energy.

Supporting Information Available: Adsorption data, detailed experimental procedures, X-ray structural data (cif file), PXRD patterns, and TGA profiles. This material is available free of charge via the Internet at http://pubs.acs.org.

JA710144K

(114) Kumar, A. V. A.; Jobic, H.; Bhatia, S. K. *J. Phys. Chem. B* **2006**, *110*, 16666–16671.
(115) Kumar, A. V. A.; Bhatia, S. K. *Phys. Rev. Lett.* **2005**, *95*, 245901-1–245901-4.
(116) Ma, S.; Zhou, H. C. *J. Am. Chem. Soc.* **2006**, *128*, 11734–11735.
(117) Basmadjian, I. D. *Can. J. Chem.* **1960**, *38*, 141–148.